Measurement of the ratio $\Gamma\_\_b\bar{b}/\Gamma\_\_had$ using event shape variables

D. Buskulic, I. de Bonis, D. Decamp, P. Ghez, C. Goy, J P. Lees, M N. Minard, B. Pietrzyk, F. Ariztizabal, P. Comas, et al.

EUROPEAN ORGANIZATION FOR NUCLEAR RESEARCH

CERN-PPE/93-113
5 July 1993

Measurement of the Ratio $\Gamma_{b\bar{b}}/\Gamma_{had}$ using Event Shape Variables

The ALEPH Collaboration*

Abstract

The branching fraction of $Z \to b\overline{b}$ relative to all hadronic decays of the Z has been measured using event shape variables to preferentially select $Z \to b\overline{b}$ events. The method chosen applies a combination of shape discriminators and the selection of high transverse momentum leptons to event hemispheres. From a sample of 440,000 hadronic Z decays collected with the ALEPH detector at LEP, the ratio $\Gamma_{b\bar{b}}/\Gamma_{had} = 0.228 \pm 0.005(stat.) \pm 0.005(syst.)$ is measured.

Submitted to Physics Letters B

*See the following pages for the list of authors

The ALEPH Collaboration

D. Buskulic, I. De Bonis, D. Decamp, P. Ghez, C. Goy, J.-P. Lees, M.-N. Minard, B. Pietrzyk

Laboratoire de Physique des Particules (LAPP), IN^{2}P^3-CNRS, 74019 Annecy-le-Vieux Cedex, France

F. Ariztizabal, P. Comas, J.M. Crespo, M. Delfino, I. Efthymiopoulos, E. Fernandez, M. Fernandez-Bosman, V. Gaitan, Ll. Garrido, T. Mattison, A. Pacheco, C. Padilla, A. Pascual

Institut de Fisica d'Altes Energies, Universitat Autonoma de Barcelona, 08193 Bellaterra (Barcelona), Spain[7]

D. Creanza, M. de Palma, A. Farilla, G. Iaselli, G. Maggi, S. Natali, S. Nuzzo, M. Quattromini, A. Ranieri, G. Raso, F. Romano, F. Ruggieri, G. Selvaggi, L. Silvestris, P. Tempesta, G. Zito

INFN Sezione di Bari e Dipartimento di Fisica dell' Università, 70126 Bari, Italy

Y. Chai, H. Hu, D. Huang, X. Huang, J. Lin, T. Wang, Y. Xie, D. Xu, R. Xu, J. Zhang, L. Zhang, W. Zhao

Institute of High-Energy Physics, Academia Sinica, Beijing, The People's Republic of China[8]

E. Blucher,[22] G. Bonvicini, J. Boudreau, D. Casper, H. Drevermann, R.W. Forty, G. Ganis, C. Gay, R. Hagelberg, J. Harvey, J. Hilgart,[31] R. Jacobsen, B. Jost, J. Knobloch, I. Lehraus, T. Lohse,[27] M. Maggi, C. Markou, M. Martinez, P. Mato, H. Meinhard, A. Minten, A. Miotto, R. Miquel, H.-G. Moser, P. Palazzi, J.R. Pater, J.A. Perlas, J.-F. Pusztaszeri, F. Ranjard, G. Redlinger,[23] L. Rolandi, J. Rothberg,[2] T. Ruan, M. Saich, D. Schlatter, M. Schmelling, F. Sefkow,[6] W. Tejessy, I.R. Tomalin, R. Veenhof, H. Wachsmuth, S. Wasserbaech,[2] W. Wiedenmann, T. Wildish, W. Witzeling, J. Wotschack

European Laboratory for Particle Physics (CERN), 1211 Geneva 23, Switzerland

Z. Ajaltouni, F. Badaud, M. Bardadin-Otwinowska, R. El Fellous, A. Falvard, P. Gay, C. Guicheney, P. Henrard, J. Jousset, B. Michel, J-C. Montret, D. Pallin, P. Perret, F. Podlyski, J. Proriol, F. Prulhière, F. Saadi

Laboratoire de Physique Corpusculaire, Université Blaise Pascal, IN^{2}P^3-CNRS, Clermont-Ferrand, 63177 Aubière, France

T. Fearnley, J.B. Hansen, J.D. Hansen, J.R. Hansen,[1] P.H. Hansen, R. Møllerud, B.S. Nilsson[1]

Niels Bohr Institute, 2100 Copenhagen, Denmark[9]

A. Kyriakis, E. Simopoulou, I. Siotis, A. Vayaki, K. Zachariadou

Nuclear Research Center Demokritos (NRCD), Athens, Greece

J. Badier, A. Blondel, G. Bonneaud, J.C. Brient, G. Fouque, S. Orteu, A. Rougé, M. Rumpf, R. Tanaka, M. Verderi, H. Videau

Laboratoire de Physique Nucléaire et des Hautes Energies, Ecole Polytechnique, IN^{2}P^3-CNRS, 91128 Palaiseau Cedex, France

D.J. Candlin, M.I. Parsons, E. Veitch

Department of Physics, University of Edinburgh, Edinburgh EH9 3JZ, United Kingdom[10]

E. Focardi, L. Moneta, G. Parrini

Dipartimento di Fisica, Università di Firenze, INFN Sezione di Firenze, 50125 Firenze, Italy

M. Corden, C. Georgiopoulos, M. Ikeda, D. Levinthal[15]

Supercomputer Computations Research Institute and Dept. of Physics, Florida State University, Tallahassee, FL 32306, USA [12,13,14]

A. Antonelli, R. Baldini, G. Bencivenni, G. Bologna,[4] F. Bossi, P. Campana, G. Capon, F. Cerutti, V. Chiarella, B. D'Ettorre-Piazzoli,[24] G. Felici, P. Laurelli, G. Mannocchi,[5] F. Murtas, G.P. Murtas, L. Passalacqua, M. Pepe-Altarelli, P. Picchi[4]

Laboratori Nazionali dell'INFN (LNF-INFN), 00044 Frascati, Italy

P. Colrain, I. ten Have, J.G. Lynch, W. Maitland, W.T. Morton, C. Raine, P. Reeves, J.M. Scarr, K. Smith, M.G. Smith, A.S. Thompson, R.M. Turnbull

Department of Physics and Astronomy, University of Glasgow, Glasgow G12 8QQ,United Kingdom[10]

B. Brandl, O. Braun, C. Geweniger, P. Hanke, V. Hepp, E.E. Kluge, Y. Maumary, A. Putzer, B. Rensch, A. Stahl, K. Tittel, M. Wunsch

Institut für Hochenergiephysik, Universität Heidelberg, 6900 Heidelberg, Fed. Rep. of Germany[16]

R. Beuselinck, D.M. Binnie, W. Cameron, M. Cattaneo, D.J. Colling, P.J. Dornan, A.M. Greene, J.F. Hassard, N.M. Lieske,[29] A. Moutoussi, J. Nash, S. Patton, D.G. Payne, M.J. Phillips, G. San Martin, J.K. Sedgbeer, A.G. Wright

Department of Physics, Imperial College, London SW7 2BZ, United Kingdom[10]

P. Girtler, D. Kuhn, G. Rudolph, R. Vogl

Institut für Experimentalphysik, Universität Innsbruck, 6020 Innsbruck, Austria[18]

C.K. Bowdery, T.J. Brodbeck, A.J. Finch, F. Foster, G. Hughes, D. Jackson, N.R. Keemer, M. Nuttall, A. Patel, T. Sloan, S.W. Snow, E.P. Whelan

Department of Physics, University of Lancaster, Lancaster LA1 4YB, United Kingdom[10]

K. Kleinknecht, J. Raab, B. Renk, H.-G. Sander, H. Schmidt, F. Steeg, S.M. Walther, R. Wanke, B. Wolf

Institut für Physik, Universität Mainz, 6500 Mainz, Fed. Rep. of Germany[16]

A.M. Bencheikh, C. Benchouk, A. Bonissent, J. Carr, P. Coyle, J. Drinkard,[3] F. Etienne, D. Nicod, S. Papalexiou, P. Payre, L. Roos, D. Rousseau, P. Schwemling, M. Talby

Centre de Physique des Particules, Faculté des Sciences de Luminy, IN^{2}P^3-CNRS, 13288 Marseille, France

S. Adlung, R. Assmann, C. Bauer, W. Blum, D. Brown, P. Cattaneo,[26] B. Dehning, H. Dietl, F. Dydak,[21] M. Frank, A.W. Halley, K. Jakobs, J. Lauber, G. Lütjens, G. Lutz, W. Männer, R. Richter, J. Schröder, A.S. Schwarz, R. Settles, H. Seywerd, U. Stierlin, U. Stiegler, R. St. Denis, G. Wolf

Max-Planck-Institut für Physik, Werner-Heisenberg-Institut, 8000 München, Fed. Rep. of Germany[16]

R. Alemany, J. Boucrot,[1] O. Callot, A. Cordier, M. Davier, L. Duflot, J.-F. Grivaz, Ph. Heusse, D.E. Jaffe, P. Janot, D.W. Kim,[19] F. Le Diberder, J. Lefrançois, A.-M. Lutz, M.-H. Schune, J.-J. Veillet, I. Videau, Z. Zhang

Laboratoire de l'Accélérateur Linéaire, Université de Paris-Sud, IN^{2}P^3-CNRS, 91405 Orsay Cedex, France

D. Abbaneo, G. Bagliesi, G. Batignani, U. Bottigli, C. Bozzi, G. Calderini, M. Carpinelli, M.A. Ciocci, R. Dell'Orso, I. Ferrante, F. Fidecaro, L. Foà, F. Forti, A. Giassi, M.A. Giorgi, A. Gregorio, F. Ligabue, A. Lusiani, E.B. Mannelli, P.S. Marrocchesi, A. Messineo, F. Palla, G. Rizzo, G. Sanguinetti, P. Spagnolo, J. Steinberger, R. Tenchini, G. Tonelli,[32] G. Triggiani, C. Vannini, A. Venturi, P.G. Verdini, J. Walsh

Dipartimento di Fisica dell'Università, INFN Sezione di Pisa, e Scuola Normale Superiore, 56010 Pisa, Italy

A.P. Betteridge, Y. Gao, M.G. Green, P.V. March, Ll.M. Mir, T. Medcalf, I.S. Quazi, J.A. Strong, L.R. West

Department of Physics, Royal Holloway & Bedford New College, University of London, Surrey TW20 OEX, United Kingdom[10]

D.R. Botterill, R.W. Clifft, T.R. Edgecock, S. Haywood, P.R. Norton, J.C. Thompson

Particle Physics Dept., Rutherford Appleton Laboratory, Chilton, Didcot, Oxon OX11 OQX, United Kingdom[10]

B. Bloch-Devaux, P. Colas, H. Duarte, S. Emery, W. Kozanecki, E. Lançon, M.C. Lemaire, E. Locci, B. Marx, P. Perez, J. Rander, J.-F. Renardy, A. Rosowsky, A. Roussarie, J.-P. Schuller, J. Schwindling, D. Si Mohand, B. Vallage

Service de Physique des Particules, DAPNIA, CE-Saclay, 91191 Gif-sur-Yvette Cedex, France[17]

R.P. Johnson, A.M. Litke, G. Taylor, J. Wear

Institute for Particle Physics, University of California at Santa Cruz, Santa Cruz, CA 95064, USA[25]

J.G. Ashman, W. Babbage, C.N. Booth, C. Buttar, S. Cartwright, F. Combley, I. Dawson, L.F. Thompson

Department of Physics, University of Sheffield, Sheffield S3 7RH, United Kingdom[10]

E. Barberio, A. Böhrer, S. Brandt, G. Cowan, C. Grupen, G. Lutters, F. Rivera,[30] U. Schäfer, L. Smolik

Fachbereich Physik, Universität Siegen, 5900 Siegen, Fed. Rep. of Germany[16]

L. Bosisio, R. Della Marina, G. Giannini, B. Gobbo, F. Ragusa[20]

Dipartimento di Fisica, Università di Trieste e INFN Sezione di Trieste, 34127 Trieste, Italy

L. Bellantoni, W. Chen, J.S. Conway,[28] Z. Feng, D.P.S. Ferguson, Y.S. Gao, J. Grahl, J.L. Harton, O.J. Hayes III, J.M. Nachtman, Y.B. Pan, Y. Saadi, M. Schmitt, I. Scott, V. Sharma, Z.H. Shi, J.D. Turk, A.M. Walsh, F.V. Weber, Sau Lan Wu, X. Wu, M. Zheng, G. Zobernig

Department of Physics, University of Wisconsin, Madison, WI 53706, USA[11]

---

[1] Now at CERN, PPE Division, 1211 Geneva 23, Switzerland.
[2] Permanent address: University of Washington, Seattle, WA 98195, USA.
[3] Now at University of California, Irvine, CA 92717, USA.
[4] Also Istituto di Fisica Generale, Università di Torino, Torino, Italy.
[5] Also Istituto di Cosmo-Geofisica del C.N.R., Torino, Italy.
[6] Now at DESY, Hamburg, Germany.
[7] Supported by CICYT, Spain.
[8] Supported by the National Science Foundation of China.
[9] Supported by the Danish Natural Science Research Council.
[10] Supported by the UK Science and Engineering Research Council.
[11] Supported by the US Department of Energy, contract DE-AC02-76ER00881.
[12] Supported by the US Department of Energy, contract DE-FG05-87ER40319.
[13] Supported by the NSF, contract PHY-8451274.
[14] Supported by the US Department of Energy, contract DE-FC05-85ER250000.
[15] Supported by SLOAN fellowship, contract BR 2703.
[16] Supported by the Bundesministerium für Forschung und Technologie, Fed. Rep. of Germany.
[17] Supported by the Direction des Sciences de la Matière, C.E.A.
[18] Supported by Fonds zur Förderung der wissenschaftlichen Forschung, Austria.
[19] Supported by the Korean Science and Engineering Foundation and Ministry of Education.
[20] Now at Dipartimento di Fisica, Università di Milano, Milano, Italy.
[21] Also at CERN, PPE Division, 1211 Geneva 23, Switzerland.
[22] Now at University of Chicago, Chicago, IL 60637, U.S.A.
[23] Now at TRIUMF, Vancouver, B.C., Canada.
[24] Also at Università di Napoli, Dipartimento di Scienze Fisiche, Napoli, Italy.
[25] Supported by the US Department of Energy, grant DE-FG03-92ER40689.
[26] Now at Università di Pavia, Pavia, Italy.
[27] Now at Max-Planck-Institut f. Kernphysik, Heidelberg, Germany.
[28] Now at Rutgers University, Piscataway, NJ 08854, USA.
[29] Now at Oxford University, Oxford OX1 3RH, U.K.
[30] Partially supported by Colciencias, Colombia.
[31] Now at SSCL, Dallas 75237-3946, TX, U.S.A.
[32] Also at Istituto di Matematica e Fisica, Università di Sassari, Sassari, Italy.

1 Introduction

Within the Standard Model of electroweak interactions, radiative corrections introduce dependence on the unknown top quark mass, m_t, into calculations of the total and partial widths of the Z boson. Corrections to the Z self energy contribute to all the partial widths through the $\Delta\rho$ parameter [1]. An additional correction modifies the $Z \rightarrow b\bar{b}$ vertex [2], so that a measurement of $\Gamma_{b\bar{b}}$ normalized to the total hadronic width Γ_{had} provides a constraint on m_t with different model-dependence to that obtained from $\Delta\rho$, and insensitive to QCD corrections. The prediction for the partial width ratio $\Gamma_{b\bar{b}}/\Gamma_{had}$ varies by over 3% when m_t varies from 80 to 260 GeV/c^2, requiring a measurement at the level of 1% precision to set meaningful constraints on the top quark mass.

Most existing experimental results on $\Gamma_{b\bar{b}}/\Gamma_{had}$ are based on the identification of the b by means of inclusive leptons [3], [4], [5]. The statistical accuracy of these methods is at present about 3.5% and is limited by the number of dilepton events. The systematic errors arise from uncertainties in semileptonic decay properties of B-hadrons: branching ratios, heavy quark fragmentation, and the shape of the lepton momentum spectrum.

An alternative approach can use all hadronic Z decays provided that the $b\overline{b}$ events can be discriminated from the light quark events ($u\bar{u}$, $d\bar{d}$, $s\bar{s}$, $c\bar{c}$) by exploiting differences in their topologies. Because of their large mass, b quarks lose less energy than lighter quarks due to gluon bremsstrahlung in the fragmentation and hadronization process. At LEP energies, B-hadrons produced in $b\overline{b}$ events carry on average 70% of the beam energy, while D-hadrons from $c\overline{c}$ events carry only 50%. The decay products of the massive B-hadrons are characterized, for example, by a higher sphericity [6]. This paper describes analyses which extract $\Gamma_{b\bar{b}}/\Gamma_{had}$ from the data by enriching the sample in $b\overline{b}$ events using estimators made up of combinations of topological variables. An analysis is presented, the 'global event method', which uses a Neural Network to combine several full event shape variables and takes the efficiency of the discriminator for $b\overline{b}$ and light quarks from Monte Carlo simulation. It is shown that this method is limited by the systematic errors on these efficiencies and a second method is introduced, the 'hemisphere method '. Here the event is split into two hemispheres and both an event shape discriminator and a high $p_\perp$ lepton tag are applied to each hemisphere to recognise $b\overline{b}$ events. By comparing the rates of events singly or doubly tagged, the efficiencies of the tags can be obtained directly from the data. The Monte Carlo is then only needed for small corrections arising from the correlations between the tags, and the overall systematic error is reduced. This method has been applied using two different event shape discriminators, one based on a likelihood built with two variables and the other formed using several variables in a Neural Network. The results of each analysis are compared and combined.

2 The ALEPH detector and event selection

The ALEPH detector has been described in detail elsewhere [7]. Here only a brief description of the parts of the apparatus relevant for this analysis are given. Charged tracks are measured over the range $|\cos\theta| < 0.966$, where θ is the polar angle, by an inner cylindrical drift chamber (ITC) and by a large cylindrical time projection chamber (TPC). These are immersed in a magnetic field of 1.5 T and together measure the momenta of charged particles with a resolution, determined from dimuon events, of $\delta p/p = p \cdot 0.0008(GeV/c)^{-1}$. The TPC also provides up to 330 measurements of the specific ionization (dE/dx) of each charged track. For electrons in hadronic events, the dE/dx resolution obtained is 4.6% for 330 ionization samples. The electromagnetic calorimeter (ECAL) is used, together with the TPC, to identify electrons. The ECAL is a lead-proportional-tube calorimeter with cathode-pad readout which has a resolution for electromagnetic showers of $\delta E/E = 0.18/\sqrt{E} + 0.01$, with E in GeV. It covers the angular region $|\cos\theta| < 0.98$ and is finely segmented into projective towers, each subtending an angle of less than 1° by 1°, which are read out in three stacks corresponding to thicknesses of 4, 9 and 9 radiation lengths. Muons are identified by the hadron calorimeter (HCAL), which is composed of the iron of the magnet return yoke interleaved with 23 layers of streamer tubes, and the muon chambers, which consist of an additional 2 double layers of streamer tubes surrounding the calorimeter. The tubes of the HCAL have a pitch of 1 cm and measure, in two dimensions, tracks from penetrating particles within the angular range $|\cos\theta| < 0.985$. The muon chambers cover the same angular range as the HCAL and provide two three-dimensional coordinates for charged tracks which penetrate the 7.5 interaction lengths of material between the chambers and the interaction point.

The selection of hadronic events is based on charged tracks. A 'good' charged track is defined as one that passes through a cylinder of 2 cm radius and 20 cm length around the interaction point, has at least four TPC coordinates, a polar angle between 18° and 162°, and a transverse momentum relative to the beam axis greater than 0.25 GeV/c. Each event is required to have at least 5 'good' charged tracks and the sum of the energies of these tracks must be greater than 10% of the center-of-mass energy. From the data taken in 1990 and 1991 a total of 437,600 events pass the selection.

Further event selections are applied for each of the analyses. First an event axis is defined for each event using all 'good' charged and neutral energy flow objects defined as in reference [8]. In the analyses using Neural Networks this axis is taken as the thrust axis and is required to lie between 30° and 150° of the beam axis. For the two variable analysis the axis is taken from the inertial matrix defined in section 3.2 and is required to lie between 32° and 148° of the beam axis. The jets of an event are reconstructed with the scaled-invariant-mass clustering algorithm [9].

For the Neural Network analyses, a further cut is imposed, requiring that the most energetic jet of the event must have at least four charged tracks or neutral energy

flow objects associated to it. After these extra cuts the selection efficiencies for the Neural Network and two variable analyses are about 80%, and the backgrounds from $\tau\bar{\tau}$ and two-photon events are $< 0.3\%$ altogether.

The Monte Carlo simulations described in this paper use the standard ALEPH event generator HVFL which is based on DYMU and JETSET 7.3 [10].

3 Event shape discriminators

3.1 Neural Network Tag

Two Neural Networks with different input variables are used for the global event shape analysis and for the hemisphere analysis. In the appendix definitions are given for the variables used as input to the two networks. These are a subsample of a larger set of variables which are discussed in detail in [11]. The quantities used were selected by applying appropriate F-Tests [12] , taking into account the correlation between the variables. For the hemisphere analysis, the observables fed to the network are computed for each hemisphere and have been chosen with the intention of reducing the correlations between the two halves of the event.

In the two analyses, 9 variables are used as inputs of a feed-forward four layer Neural Network, the structure of which is the following: one input layer with 9 neurons, two hidden layers with 9 and 6 neurons respectively, and one final layer with 1 neuron giving the output of the network. The number of hidden layers and the number of neurons per layer have been chosen to optimize the separation between b and non-b events. Each neuron of a given layer is connected to all the neurons of the following layer. To each connection is associated a weight W which is determined during the learning phase. More technical details can be found in [11].

For the training of the two networks, 9000 $b\overline{b}$, 9000 $c\overline{c}$ and 9000 $u\bar{u}$, $d\bar{d}$, $s\bar{s}$ simulated events were used. One event of each class is presented to the network. The obtained output is then compared to the desired value (1 for $b\overline{b}$ events and 0 otherwise) and the recalculation of the weights W is made accordingly, after one exposure of an event of each class, by using a gradient descent method with backpropagation of the errors [11].

Checks have been made that the relative fractions of b and $udsc$ quarks in the learning set and the order in which each class of events is presented do not bias the result of the training. The efficiency of the algorithm has been estimated with a sample of about 200,000 simulated hadronic Z decays, different from those of the learning sample. For each $q\bar{q}$ event the discriminator output obtained with the Neural Network has been computed. Cuts on this discriminator output provide enriched samples in $b\overline{b}$ events. For instance, a b-purity of 52% for the event tag and of 36% for the hemisphere tag can be obtained for a b-efficiency of 75%.

3.2 Two variable tag

For the two variable double tag method two additional hemisphere shape variables have been defined. The variables are computed taking all selected neutral and charged tracks as the particles of the event. The event axis for this analysis is obtained from an inertial matrix defined by:

$$\lambda_{ij} = \sum_{m=1}^{n} \frac{-p_m^i p_m^j}{|\vec{p}_m|},$$

and

$$\lambda_{kk} = \sum_{m=1}^{n} \frac{(p_m^i)^2 + (p_m^j)^2}{|\vec{p}_m|}, k \neq i, j,$$

where p_m^i is the ith component of the momentum vector of the mth particle, and i, j, k run over the three Cartesian coordinates. The first eigenvector of this matrix filled with all particles in the event is taken as the event axis for this analysis (omitting the $|\vec{p}_m|$ in the denominator of the entries would give the sphericity axis). Each event is divided into hemispheres using the plane perpendicular to the event axis, and a hemisphere axis is calculated in the same way as the event axis, but using only tracks in the same hemisphere. Then, aiming to reduce the correlations between the hemispheres, only particles with momenta making an angle of less than 45° with the hemisphere axis are used to calculate the variables.

The two shape variables were computed separately for each hemisphere using the momenta of the particles boosted into the rest frame defined by the sum of the momenta of all selected particles in that hemisphere. Although b jets have on average a similar mass to light quark jets, the total momentum in the center of mass frame of the jet is on average more uniformly distributed among the constituents. Therefore one of the quantities used is the 'moment of inertia', defined as the first eigenvalue of the inertial matrix for each hemisphere, normalized to the sum of all three eigenvalues. This is related to boosted sphericity but is obtained with variable boost, and is weighted linearly rather than quadratically in momentum. The distribution of this quantity is shown in figure 1a for simulated b, c and light quarks events. The second variable used is the 'lateral mass', which is intended to distinguish between products of gluon bremsstrahlung and decay products in the final state from their direction relative to the boost of the jet. It is defined as the sum of the boosted momenta of those particles in the hemisphere that make an angle with the hemisphere axis such that $|cos\theta| < .75$. The distributions of lateral mass for different species in Monte Carlo data are shown in figure 1b. To combine the two variables into a single estimator the likelihood that a hemisphere with a given lateral mass and moment of inertia was due to a $Z \to b\bar{b}$ event was determined using the Monte Carlo simulation. For the cut of 0.28 on this likelihood chosen for the hemisphere analysis described later, the b tag efficiency is 73% with a b purity of 36%.

4 The High $p_\perp$ Lepton Tag

The hemisphere method uses a high $p_\perp$ lepton tag to measure the efficiency of the event shape discriminators. Leptons are identified using standard ALEPH algorithms [13]. Muons and electrons are both required to have momenta greater than 3 GeV/c. The same methods as described in reference [13] are used to reject photon conversions and Dalitz pairs. The lepton is assigned to one of the two hemispheres of the event using the appropriate event axis defined above. A lepton is only used if it is assigned to a jet with at least two additional particles, and the lepton transverse momentum is calculated relative to the jet's momentum after first subtracting the lepton momentum from that of the jet. Any hemisphere containing at least one lepton with transverse momentum greater than 1.25 GeV/c is used in the lepton sample.

For the hemisphere double tag method, knowledge is needed of the hemisphere b-purity in the lepton sample, $f_b^L = N_b/(N_b + N_c + N_{uds})$, where N_b, N_c and N_{uds} are the number of hemispheres containing a high $p_\perp$ lepton candidate from $b\bar{b}$, $c\bar{c}$ and light quark events. The contributions from $b\overline{b}$ and $c\overline{c}$ events are experimentally determined on the basis of a global fit to the p and $p_\perp$ spectra of single and dilepton events [4], extracting $\Gamma_{b\bar{b}}/\Gamma_{had}$, $\Gamma_{c\bar{c}}/\Gamma_{had}$, $BR(b \to l)$, $BR(b \to c \to l)$ and the b and c-fragmentation parameters. Once the parameters are known on the basis of the full $p_\perp$ analysis, the contributions of the various lepton sources can then be computed in any restricted $p_\perp$ region.

The dominant systematic uncertainties in f_b^L come from the modelling of b and c semileptonic decays. For primary b decays two models, ACCMM [14] and ISGW [15] are used which fit the available lepton spectra for B's from $\Upsilon(4S)$ decay. They differ in the relative hardness of the spectra and the systematic uncertainty is taken as half the purity difference obtained with the two models. For the shape of the $c \to l$ spectrum, half of the difference between the DELCO results at the ψ'' and the predictions of JETSET are taken. Modelling of the $b \to c \to l$ spectrum is more complex as fewer data are available. Conservatively the total difference between the JETSET values and JETSET suitably modified with the $c \to l$ corrections is used for the error. This leads to a contribution to the systematic error of 0.47%; lepton identification efficiencies and backgrounds (evaluated from the data) bring the total systematic error to 0.55%. The statistical error on f_b^L is that of the fit, taking into account the correlations between the different parameters. For the chosen cut, $p_\perp > 1.25$ GeV/c, the purity of the lepton sample is:

$$f_b^L = 0.8829 \pm 0.0050(stat.) \pm 0.0055(syst.). \qquad (1)$$

The analysis used to obtain this purity also gives a measurement of $\Gamma_{b\bar{b}}/\Gamma_{had}$ and will soon be published in detail [3]. The correlation between the value $\Gamma_{b\bar{b}}/\Gamma_{had}$ obtained from this fit and f_b^L is taken into account and contributes $\pm 0.21\%$ to the statistical error on f_b^L.

5 Measurement of $\Gamma_{b\bar{b}}/\Gamma_{had}$

5.1 The global event method

A conventional method to measure the b fraction in hadronic events is based on global event shape analysis [16]. This is statistically powerful but the systematic uncertainty is large due to a strong dependence on fragmentation. A similar analysis has been performed using Neural Network techniques and is described in the following.

The shape of the discriminator output for b and light quark events are parametrized by using a large sample of simulated events. These functions $\mathcal{F}_b$ and $\mathcal{F}_{udsc}$ are normalized and the Neural Network output corresponding to the data, $\mathcal{F}_{data}$, is fitted according to the formula:

$$\mathcal{F}_{data} = N_b \mathcal{F}_b + (N_{had.} - N_b)\mathcal{F}_{udsc} \tag{2}$$

where $N_{had.}$ is the number of hadronic events and N_b is the free parameter of the fit. Fig. 2 shows the shape of the discriminator output of Neural Network obtained for data and Monte Carlo. The Monte Carlo gives a good description of the data. The resulting fitted value is:

$$\Gamma_{b\bar{b}}/\Gamma_{had} = N_b/N_{had.} = 0.214 \pm 0.002(stat.).$$

This result has been obtained by using the average values $< X_b >= 0.719 \pm 0.012$ and $< X_c >= 0.495 \pm 0.011$ [17, 18], where X_b and X_c are defined to be the ratio of the B- and D-hadron energy to the beam energy.

Source	parameter variation	Effect on $\Gamma_{b\bar{b}}/\Gamma_{had}$
$< X_b >$	0.707 - 0.731	$\pm$0.0031
$< X_c >$	0.484 - 0.506	$\pm$0.0020
$\Gamma_{c\bar{c}}/\Gamma_{had}$	0.15 - 0.19	$\pm$0.0016
Λ_{LLA}	0.28 - 0.35 GeV	$\pm$0.0057
M_{min}	1.0 - 1.8 GeV	$\pm$0.0027
$\sigma_\perp$	0.34 - 0.38 GeV	$\pm$0.0016
b	0.80 - 1.00 GeV^{-2}	$\pm$0.0045
s/u	0.20 - 0.40	$\pm$0.0015
$V/(V+P)$	0.25 - 0.80	$\pm$0.0028
MC statistics		$\pm$0.0022
HERWIG		$\pm$0.0077
Total		$\pm$0.0124

Table 1: Sources of systematic errors and their contributions to the error on $\Gamma_{b\bar{b}}/\Gamma_{had}$.

Systematic errors are determined by varying the heavy quark fragmentation parameters, the $c\bar{c}$ partial width, QCD parameters Λ_{LLA}, M_{min}, $\sigma_\perp$ and b, within their errors [20], and the JETSET parameters s/u and $V/(V+P)$ as described in [21] [†]. The influence of the QCD parameters has been studied by varying each parameter in turn by twice its error and determining the new central values of the three others as explained in [20]. It has been verified that the extraction of the QCD parameters in this reference is not sensitive to large variations of $\Gamma_{b\bar{b}}/\Gamma_{had}$ and therefore does not constitute a bias for this analysis. These contributions to the systematic error are shown in table 1. The analysis was repeated using the HERWIG Monte-Carlo and the difference was taken as a systematic error.

Adding the systematic errors in quadrature the result of this global event analysis is:

$$\Gamma_{b\bar{b}}/\Gamma_{had} = 0.214 \pm 0.002(stat.) \pm 0.012(syst.).$$

This result is statistically powerful, but relies on Monte Carlo simulation to describe the shape of b and $udsc$ quark events and therefore results in large and uncertain systematic errors. A new method has therefore been developed which is less model dependent.

5.2 The hemisphere method

This new analysis has been performed with both the Neural Network and the two variable event shape discriminators. The events are split into two hemispheres according to the plane perpendicular to the event axis and the event shape discriminators and the high $p_\perp$ lepton discriminators are applied to each hemisphere.

For a given cut on the event shape discriminator, 3 samples are defined: a class of hemispheres satisfying the cut ('tagged hemispheres'), a class where both hemispheres of an event satisfy the cut ('double tagged events') and a class of events tagged by a high $p_\perp$ lepton on one side and the event shape discriminator on the other side ('single tagged high $p_\perp$ leptons'). Then it is possible to extract from the data the efficiencies of the event shape tag, ϵ_b and ϵ_{udsc} for b and $udsc$ hemispheres, and the fraction of $b\bar{b}$ events in the hadronic sample, f_b. This is achieved by solving the following system of equations,

$$\left\{ \begin{array}{l} N^{ST}/2N_{had.} = f_b\epsilon_b + (1-f_b)\epsilon_{udsc} \\ N^{DT}/N_{had.} = f_b\epsilon_b^2(1+C_b^D) + (1-f_b)\epsilon_{udsc}^2(1+C_{udsc}^D+K_{udsc}^D) \\ N_{lept.}^{ST}/N_{lept.} = f_b^L\epsilon_b(1+C_b^L) + (1-f_b^L)\epsilon_{udsc}(1+C_{udsc}^L+K_{udsc}^L) \end{array} \right. \quad (3)$$

where:

[†] Λ_{LLA} is the QCD scale parameter used in running α_s, M_{min} is the mass cutoff below which the partons of the parton shower are not assumed to radiate, $\sigma_\perp$ is the width of the Gaussian transverse momentum distributions of primary hadrons and b is the parameter of the symmetric Lund fragmentation function; s/u is the relative probability to create an $s\bar{s}$ pair from the vacuum compared to $u\bar{u}$ pairs and $V/(V+P)$ is the ratio of vector to vector plus pseudoscalar mesons.

– f_b^L is the hemisphere b-purity in the high $p_\perp$ lepton sample which is determined by the fit described in section 4.

– N^{ST}, N^{DT} and $N^{ST}_{lept.}$ are the number of "tagged hemispheres", "double tagged events" and "single tagged high $p_\perp$ leptons", respectively. $N_{had.}$ and $N_{lept.}$ are the total number of hadronic events and high $p_\perp$ lepton tagged hemispheres used for this analysis.

– C_b^D and C_{udsc}^D are correction factors which take into account correlations between the two hemispheres due to kinematical constraints (conservation of momentum for instance). They are defined by the following relation:

$$C_i^D = \frac{\epsilon_i^{DT} - \epsilon_i^2}{\epsilon_i^2} \qquad with\ i = b,\ udsc. \tag{4}$$

where ϵ^{DT} is the probability that both hemispheres of an event satisfy the cut on the event shape discriminator ($\epsilon^{DT} = N^{DT}/N_{had.}$ for $q\bar{q}$ events).
These two coefficients are determined by using more than one million reconstructed hadronic Monte Carlo events. The values for the coefficient C_{udsc}^D were obtained for $c\bar{c}$ and uds events independently.

– C_b^L and C_{udsc}^L are correction factors which take into account possible correlations between the two hemispheres due to the identification of a high $p_\perp$ lepton, with missing energy carried out by the neutrino, in the opposite hemisphere. They are defined by the following relation:

$$C_i^L = \frac{\epsilon_i^{lepton} - \epsilon_i}{\epsilon_i} \qquad with\ i = b,\ udsc. \tag{5}$$

where ϵ^{lepton} is the probability to tag the hemisphere opposite to the high $p_\perp$ lepton ($\epsilon^{lepton} = N^{ST}_{lept.}/N_{lept.}$ for $q\bar{q}$ events). These two coefficients are consistent with zero in the Monte Carlo. They have been determined in the same way as C_b^D and C_{udsc}^D by using large samples of reconstructed hadronic Monte Carlo events.

– K_{udsc}^D and K_{udsc}^L are corrections accounting for a higher hemisphere tagging efficiency for charm events ϵ_c than for uds events ϵ_{uds} (see figure 3). For example, for a cut at 0.3 on the Neural Network output, Monte Carlo predictions give: $\epsilon_c = 0.4309 \pm 0.0009$ and $\epsilon_{uds} = 0.3670 \pm 0.0005$ leading to $\epsilon_{udsc} = 0.3811 \pm 0.0004$, where the errors are due to our Monte Carlo statistics. These two correction coefficients depend on the fractions f_c and f_c^L of $c\bar{c}$ events in the non-b hadronic and leptonic samples respectively and are given by the following equations:

$$K_{udsc}^D = \frac{(1 - f_c) f_c (\epsilon_c - \epsilon_{uds})^2}{\epsilon_{udsc}^2} \tag{6}$$

$$K_{udsc}^L = \frac{(f_c^L - f_c)(\epsilon_c - \epsilon_{uds})}{\epsilon_{udsc}}. \tag{7}$$

The charm fractions are determined by the multi-lepton fit and the values used are: $f_c = 0.21 \pm 0.02$ and $f_c^L = 0.57 \pm 0.07$ [3]. For a given cut on the event shape discriminator, ϵ_c and ϵ_{uds} are estimated from Monte Carlo and the two coefficients K^L_{udsc} and K^D_{udsc} calculated. The systematic uncertainty on ϵ_c was obtained by varying the Petersen fragmentation parameter for charm within the range .040 to .066 as indicated from a study of D* production [18].

The method has been applied in two independent analyses using the two different event shape tags and with the same high $p_\perp$ lepton tag. The cuts on the two event shape discriminators and on the $p_\perp$ of the leptons were chosen to minimize the combined statistical and systematic errors on the result and in both cases the optimal cut gives the b-tag efficiency, ϵ_b, about 75%. The correction coefficients were separately calculated from the Monte Carlo and table 2 lists the correction coefficients used for the two analyses. In order to derive the value of $\Gamma_{b\bar{b}}/\Gamma_{had}$ from the measurement of f_b, it is necessary to take into account the difference of acceptance between $b\bar{b}$ events and all hadronic events. Table 2 gives this correction, Δ_{acc} defined as the ratio of the acceptance of $b\bar{b}$ events to all $q\bar{q}$ events, which is obtained from the Monte Carlo; the correction is higher for the Neural Network analysis due to the additional event selection cut described in section 2. The results for the two analyses are given in table 3. The Neural Network analysis has a higher efficiency for a given b-purity and this leads to a slightly improved statistical error on $\Gamma_{b\bar{b}}/\Gamma_{had}$.

Parameter	Parameter value		Correction factor on $\Gamma_{b\bar{b}}/\Gamma_{had}$	
	Two Variables	Neural Network	Two Variables	Neural Network
C^D_{udsc}	0.009 ± 0.0014	0.033 ± 0.0020	0.967	0.915
C^D_b	0.003 ± 0.001	0.001 ± 0.001	0.988	0.997
C^L_{udsc}	0.007 ± 0.015	-0.001 ± 0.016	1.002	1.000
C^L_b	-0.001 ± 0.001	-0.001 ± 0.001	0.996	0.996
K^D_{udsc}	0.004 ± 0.002	0.005 ± 0.002	0.983	0.989
K^L_{udsc}	0.061 ± 0.015	0.060 ± 0.015	1.017	1.014
Δ_{acc}	1.002 ± 0.001	1.013 ± 0.002	0.998	0.987

Table 2: Correction coefficients from Monte Carlo for the two analyses with the different event shape discriminators. Note that the errors on the corrections coefficients are statistical except for K^D_{udsc} and K^L_{udsc} where the errors are systematic.

Taking into account the statistical correlation between the analyses, which is 66%, the two results are in agreement and they are combined using the procedure of reference [22], to yield the value $\Gamma_{b\bar{b}}/\Gamma_{had} = 0.228 \pm 0.005$.

To check the stability of the result for $\Gamma_{b\bar{b}}/\Gamma_{had}$, the analyses have been repeated using different cuts on their respective event shape discriminators, for $p_\perp^{lepton} > 1.25$ GeV/c. The resulting values of $\Gamma_{b\bar{b}}/\Gamma_{had}$ are plotted in figure 4a as a function of ϵ_b

for each cut. The lepton $p_\perp$ requirement has also been varied, with the discriminator cuts set to the chosen value of each analysis, as shown in figure 4b. These checks show that the determination of $\Gamma_{b\bar{b}}/\Gamma_{had}$ is independent of the cuts within the errors.

Both analyses have been checked with Monte Carlo events and the results are summarized in table 3. This table also shows the efficiencies, ϵ_b and ϵ_{udsc}, which are obtained from the data. While for the Neural Network analysis these efficiencies are the same for data and Monte Carlo, there is a significant difference in the efficiencies for the Two Variable analysis, indicating that the variables used are not well described by the simulation. Since the nature of the method is to obtain these efficiencies from the data the result is not affected by this discrepency.

analysis	parameter	Data	MC True	MC Extracted
Two Variables	ϵ_b	0.725 ± 0.004	0.747	0.745 ± 0.003
	ϵ_{udsc}	0.390 ± 0.002	0.421	0.421 ± 0.002
	$\Gamma_{b\bar{b}}/\Gamma_{had}$	0.2292 ± 0.0061	0.219	0.221 ± 0.005
Neural Network	ϵ_b	0.762 ± 0.004	0.751	0.752 ± 0.002
	ϵ_{udsc}	0.380 ± 0.002	0.381	0.381 ± 0.002
	$\Gamma_{b\bar{b}}/\Gamma_{had}$	0.2274 ± 0.0054	0.219	0.221 ± 0.004

Table 3: Results on the ratio $\Gamma_{b\bar{b}}/\Gamma_{had}$ for the two hemisphere analyses together with efficiencies for tagging b and $udsc$ events as extracted from the data. Also shown are the results of tests of the analyses on simulated events. The 'MC True' values are obtained knowing the true flavour of the generated events in the sample and the 'MC Extracted' values are obtained using the analysis methods as applied to the data.

The main systematic errors in the measurement arise from the uncertainties in the purity f_b^L of the high $p_\perp$ lepton tag and in the correction factors C_{udsc}^L, C_b^D, C_{udsc}^D and C_b^L. The contributions from the different sources of systematic error are listed in table 4. The uncertainties in the correction coefficients $C_{b,udsc}^{D,L}$, are dominated by Monte Carlo statistics; varying input parameters to the Monte Carlo within the ranges in table 1 leads to much smaller systematic effects than this level of statistical precision. For example, the largest effect identified is from b fragmentation where the systematic is one half the statistical error. The effect of each correction coefficient is shown in table 2. Uncertainties in the coefficients K_{udsc}^D and K_{udsc}^L result from uncertainties in ϵ_c, f_c and f_c^L as in equations 6 and 7. These K coefficients produce anticorrelated and nearly cancelling changes in $\Gamma_{b\bar{b}}/\Gamma_{had}$ and so the sensitivity to these parameters is diminished.

The systematic errors for the two analyses are highly correlated and the combined systematic error is taken as an average, giving the result of the combined analysis as

$$\Gamma_{b\bar{b}}/\Gamma_{had} = 0.228 \pm 0.005(stat.) \pm 0.005(syst.)$$

Source	Two Variables	Neural Network
f_b^L	± 0.0037	± 0.0037
C_b^D	± 0.0011	± 0.0010
C_{udsc}^D	± 0.0013	± 0.0016
C_b^L	± 0.0010	± 0.0010
C_{udsc}^L	± 0.0011	± 0.0010
ϵ_c	± 0.0008	± 0.0008
f_c	± 0.0005	± 0.0005
f_c^L	± 0.0006	± 0.0006
backgrounds	± 0.0006	± 0.0001
geometrical effects	± 0.0007	± 0.0007
acceptance	± 0.0002	± 0.0004
Total	± 0.0046	± 0.0046

Table 4: Contributions to the systematic error on $\Gamma_{b\bar{b}}/\Gamma_{had}$.

6 Conclusion

The ratio $\Gamma_{b\bar{b}}/\Gamma_{had}$ has been measured using analyses based on event shape variables. An analysis applying a Neural Network to the global events shape is found to suffer from large systematic uncertainties due to the fragmentation process. As a consequence a new method has been developed, where each event is split into two hemispheres and the discrimination between Z decays into b quarks and light quarks is obtained using both event shape discriminators and a high $p_\perp$ lepton tag. This procedure has been applied using two different shape discriminators, one based on a Neural Network and the other on a likelihood built from two variables. The two analyses give consistent results and have been combined, giving the result:

$$\Gamma_{b\bar{b}}/\Gamma_{had} = 0.228 \pm 0.005(stat.) \pm 0.005(syst.).$$

Because of the uncertainties in its systematic error the result from the global event method is not included in this average.

Acknowledgement

We would like to thank our colleagues of the CERN accelerator divisions for the excellent performance of the LEP accelerator. Thanks are also due to the many engineering and technical personnel at CERN and at the home institutes for their contributions toward the success of ALEPH. Those of us not from member states wish to thank CERN for its hospitality.

Appendix – Definitions of the Neural Network Variables

Only brief descriptions are given here of the event shape variables used in the Neural Network. Details can be found in [11] and in the references given below.

A) Variables for Neural Network of global event method

• A(1) is the Boosted Jet Sphericity Product. Instead of the hemispheres the two most energetic jets of the event are boosted with $\beta_{boost} = 0.965$ [6].
• A(2) and A(3) are respectively the third and fifth Fox-Wolfram-Moments [23] normalized to the 0^{th} moment.
• A(4) is the momentum of the leading particle of the event normalized to the sum of the momenta of the selected particles (P_{total}).
• A(5) is the sum of the momentum components perpendicular to the event plane of the selected particles normalized to P_{total} [19].
• A(6) is the transverse mass of the event [24].
• A(7) is the mass of the most energetic jet of the event.
• A(8) is the sum of the squared transverse momentum of the particles in the jet with respect to the jet axis of the most energetic jet of the event.
• A(9) is the transverse momentum of the leading particle of the energetic jet of the event with respect to the jet axis.

B) Variables for Neural Network of hemisphere method

• B(1) is the same as A(8) but for the most energetic jet of the hemisphere.
• B(2) and B(3) are the longitudinal momentum of the leading and of the second leading particle of the most energetic jet of the hemisphere with respect to the jet axis.
• B(4) is the boosted sphericity ($\beta_{boost} = 0.965$) of the most energetic jet of each hemisphere.
• B(5) is the product of the sum of the transverse momenta by the sum of the longitudinal momenta normalized to P_{total}^2 where P_{total} is the sum of the momentum of all the tracks of the hemisphere.
• B(6) is the invariant mass of the three most energetic particles of the most energetic jet [25].
• B(7), B(8) and B(9) are the directed sphericities described in [25].

References

[1] M. Veltman, Nucl. Phys. **B123** (1977) 89.

[2] A. A. Akhundov, D. Yu Bardin and T. Riemann, Nucl. Phys. **B276** (1986) 1.
J. Bernabéu, A. Pich and A. Santamaria, Phys. Lett. **B200** (1988) 569.
W. Beenakker and W. Hollik, Z. Phys. **C40** (1988) 141.

B. W. Lynn and R. G. Stuart, Phys. Lett. **B252** (1990) 676.
J. Bernabéu, A. Pich and A. Santamaria, Nucl. Phys. **B363** (1991) 326.

[3] D. Buskulic *et al.*, ALEPH Collab., *Heavy Flavour Quark Production and Decay using Prompt Leptons in the ALEPH Detector*, in preparation.

[4] P. Perret, ALEPH Collab.,*Precision Measurements of* $\Gamma(Z \to b\bar{b})$, presented at La Thuile, Aosta Valley, March 7-13 1993, LPC preprint PCCF RI 9313.

[5] P. D. Acton *et al* OPAL Collab., CERN PPE/93-46 (1993).
B. Adeva *et al.*, L3 Collab., Phys. Lett. 261B (1991) 177.
P. Abreu *et al*, DELPHI Collab., Z. Phys. C56 (1992) 47.

[6] W. Braunschweig *et al.*, TASSO Collab., Z. Phys. **C44** (1989) 1.

[7] D. Decamp *et al.*, ALEPH Collab., Nucl. Inst. and Meth. **A294** (1990) 121.

[8] D. Decamp *et al.*, ALEPH Collab., Phys. Lett. **B246** (1990) 306.

[9] W. Bartel *et al.*, JADE Collab., Z. Phys. **C33** (1986) 23.
S. Bethke *et al.*, JADE Collab., Phys. Lett. **B213** (1988) 235.

[10] J. E. Campagne and R. Zitoun, Z. Phys. **C43** (1989) 469.
T. Sjöstrand and M. Bengtsson, Comp. Phys. Com. **43** (1987) 367.

[11] J. Proriol et al., *Neural Network: from biology to High Energy Physics*, editors: O. Benhar et al., Ets. Editrice Pisa (1992).

[12] M.S. Srivastava and E.M. Carter, *An introduction to applied multivariate statistics*, North-Holland Amsterdam (1983).

[13] D. Decamp *et al.*, ALEPH Collab., Phys. Lett. **B244** (1990) 551,
D. Decamp *et al.*, ALEPH Collab., Phys. Lett. **B263** (199 1) 325.

[14] G. Altarelli *et al.*, Nucl Phys. B208 (1982) 365.

[15] B. Grinstein *et al.*, Phys. Rev. Lett. 56 (1986) 298.
B. Grinstein *et al.*, Phys. Rev. D 39 (1989) 799.

[16] B. Adeva *et al*, L3 Collab., CERN-PPE/93-60 (1993)
P. Abreu *et al*, DELPHI Collab., Phys. Lett. 295B (1992) 383.

[17] D. Decamp *et al.*, ALEPH Collab., *Heavy Flavour Physics with Leptons*, Contributed paper to the $XXVI^{th}$ International Conference on High Energy Physics, 6-12 August 1992, Dallas.

[18] D. Decamp *et al.*, ALEPH Collab., *Production of Charmed Mesons in Z decays*, Contributed paper to the $XXVI^{th}$ International Conference on High Energy Physics, 6-12 August 1992, Dallas.

[19] B. Brandl, University of Heidelberg preprint HD-IHEP 91-7.
B. Brandl, ALEPH Coll., XXVIIth Rencontres de Moriond on *Electroweak Interactions and Unified Theories*, March 15-22, 1992.

[20] D. Buskulic *et al.*, ALEPH Collab., Z. Phys. **C55** (1992) 209.

[21] D. Decamp *et al.*, ALEPH Collab., Phys. Lett. 259B (1991) 377.

[22] L. Lyons, et al., Nucl. Inst. and Meth. **A270** (1988) 110.

[23] G. C. Fox, S. Wolfram, Phys. Rev. Lett. **23** (1978) 1581 and Nucl. Phys. **B149** (1979) 413.

[24] W. Bartel *et al.*, JADE collab., Phys. Lett. 146B (1984) 437.

[25] L. Bellantoni, J. S. Conway, J. E. Jacobsen, Y. B. Pan, Sau Lan Wu, Nucl. Inst. and Meth. **A310** (1991) 618.

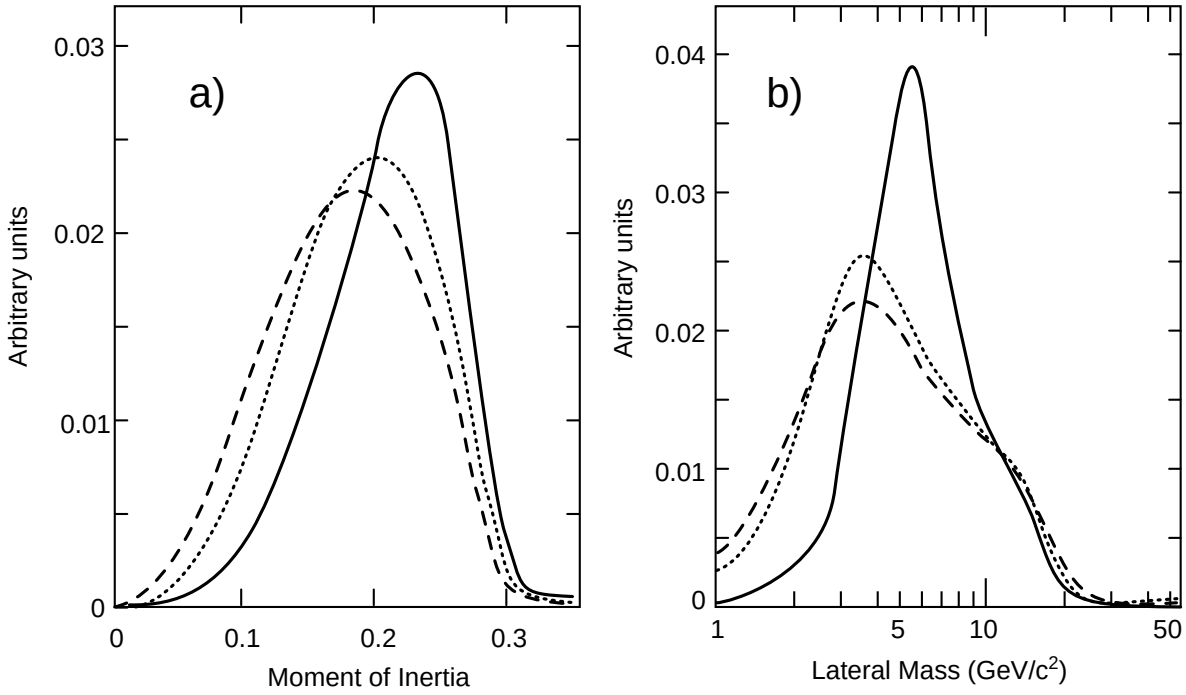

Figure 1: Distributions of quantities used in the two variable hemisphere method, (a) Lateral mass variable, (b) Moment of inertia variable, for different flavour Monte Carlo events: b solid line, c dotted, uds dashed. (All curves are normalised to have the same area.)

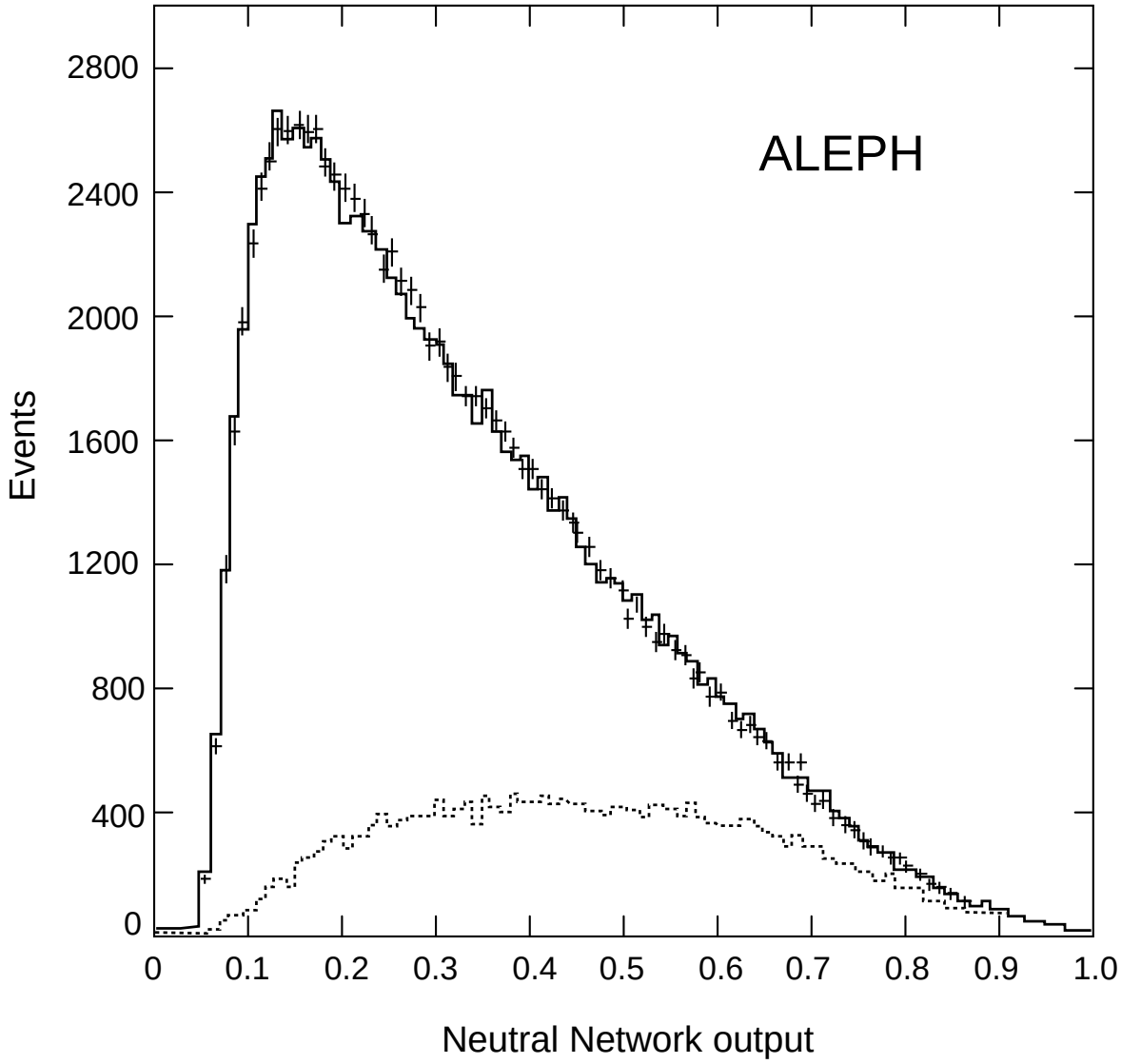

Figure 2: Shape of the Neural Network discriminator output for the Global Event analysis, for data (points) and full $q\bar{q}$ Monte Carlo (solid histogram) with the contribution from $b\bar{b}$ (dotted histogram).

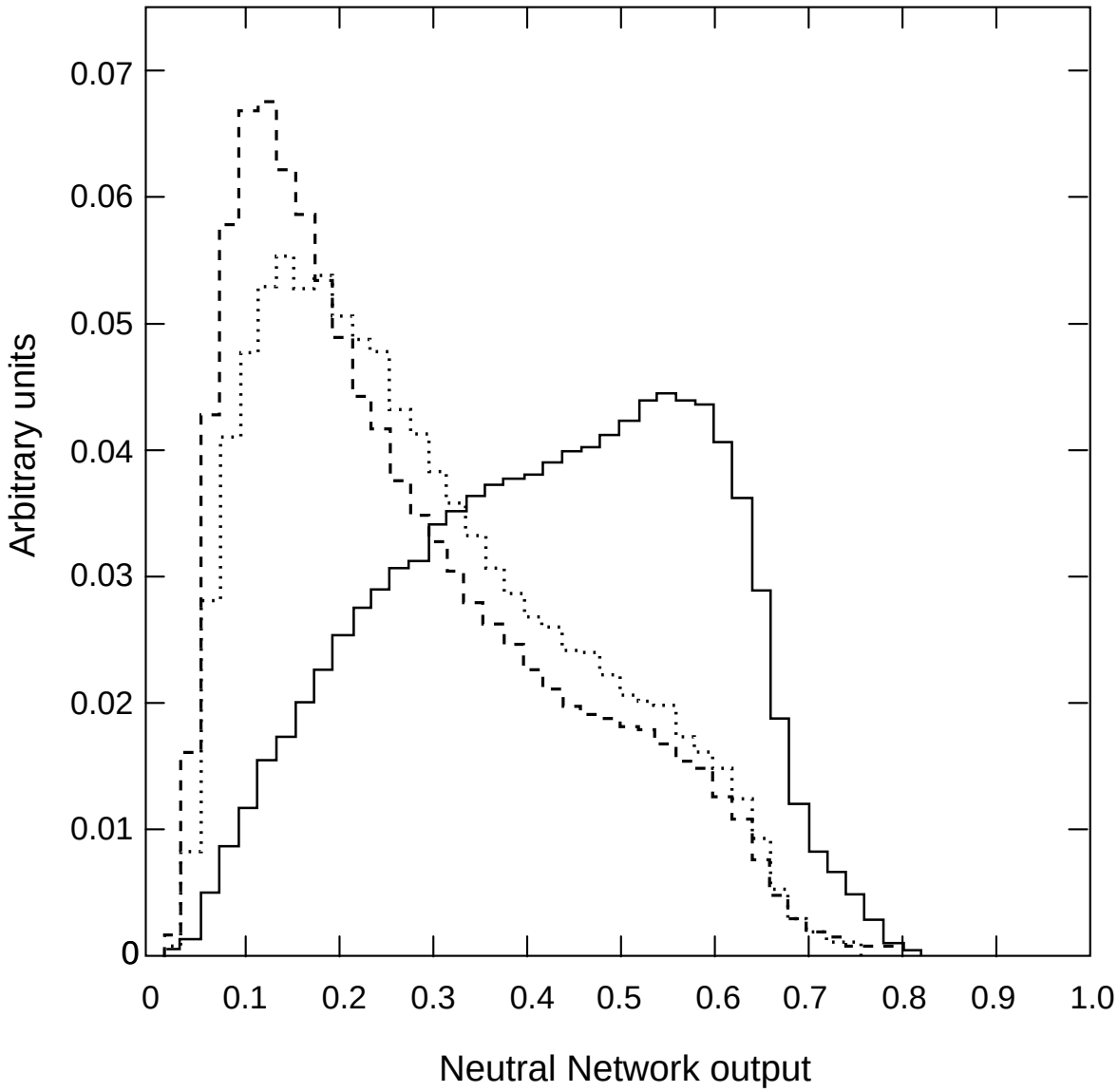

Figure 3: Neural Network output from the hemisphere method: $b\bar{b}$ Monte Carlo (solid histogram), $c\bar{c}$ Monte Carlo (dotted histogram) uds Monte Carlo (dashed histogram).

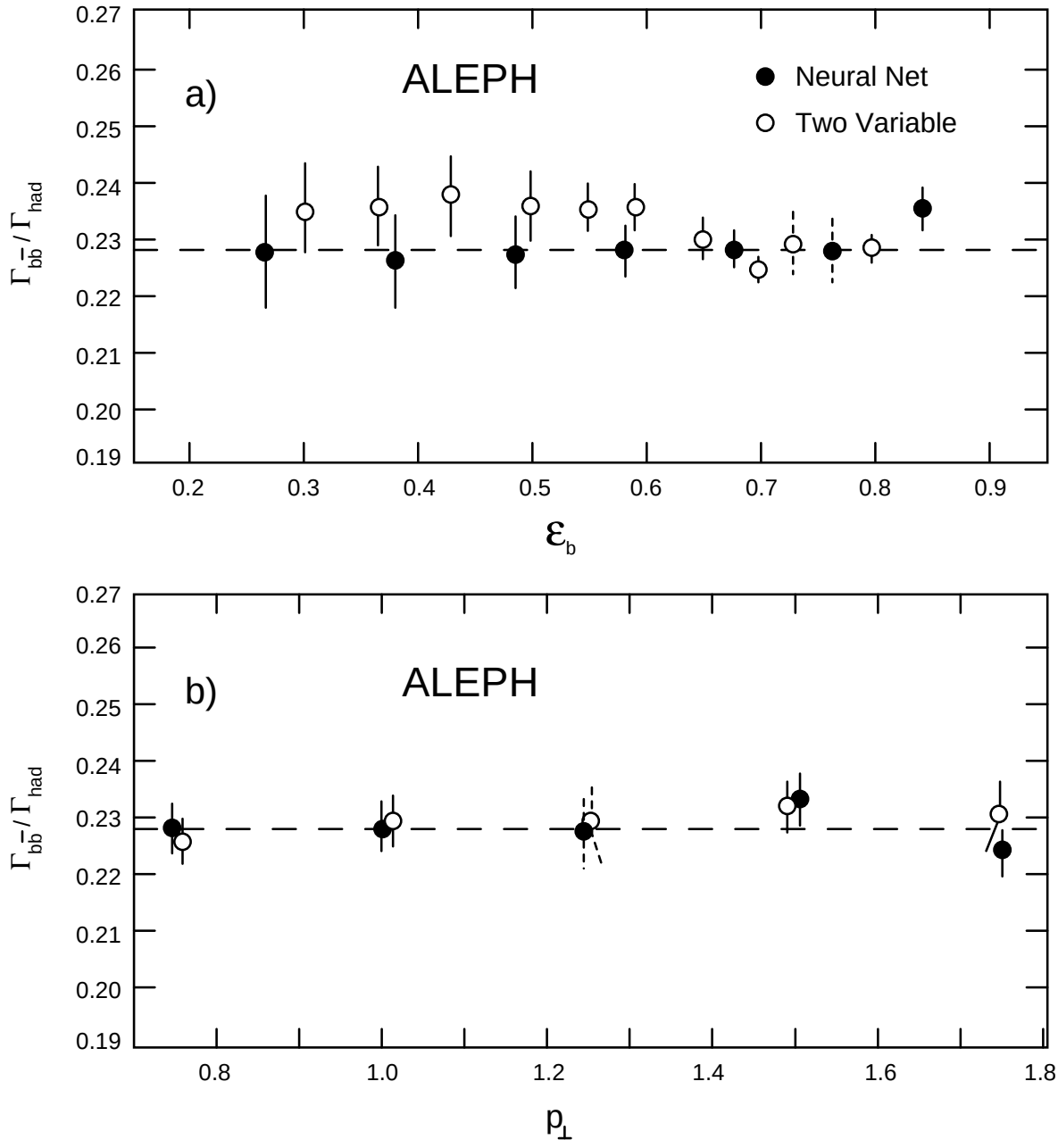

Figure 4: Results on $\Gamma_{b\bar{b}}/\Gamma_{had}$ for the two analyses a) for different cuts on the Neural Network output and on the hemisphere likelihood for $p_\perp^{lepton} > 1.25$ GeV/c, b) for different cuts on $p_\perp^{lepton}$ with a cut at 0.3 on the Neural Network output and 0.28 on the hemisphere likelihood. The points with dashed error bars are those with the standard cuts and these error bars show the total statistical error. The points for other cuts have statistical errors for the difference relative to the standard cut points.